Simultaneous measurement of thermal diffusivity and optical absorption coefficient using photothermal radiometry. II Multilayered solids

Agustín Salazar,[1,a)] Raquel Fuente,[1] Estibaliz Apiñaniz,[1] Arantza Mendioroz,[1] and R. Celorrio[2]
[1]*Departamento de Física Aplicada I, Escuela Técnica Superior de Ingeniería, Universidad del País Vasco, Alameda Urquijo s/n, Bilbao 48013, Spain*
[2]*Departamento de Matemática Aplicada, EINA/IUMA, Universidad de Zaragoza, Campus Río Ebro, Edificio Torres Quevedo, Zaragoza 50018, Spain*

(Received 7 April 2011; accepted 11 June 2011; published online 9 August 2011)

The aim of this work is to analyze the ability of modulated photothermal radiometry to retrieve the thermal diffusivity and the optical absorption coefficient of layered materials simultaneously. First, we extend the thermal quadrupole method to calculate the surface temperature of semitransparent multilayered materials. Then, this matrix method is used to evaluate the influence of heat losses by convection and radiation, the influence of the use of thin paint layers on the accuracy of thermal diffusivity measurements, and the effect of lateral heat diffusion due to the use of Gaussian laser beams. Finally, we apply the quadrupole method to retrieve (a) the thermal contact resistance in glass stacks and (b) the thermal diffusivity and optical absorption coefficient depth profiles in heterogeneous materials with continuously varying physical properties, as is the case of functionally graded materials and partially cured dental resins. © *2011 American Institute of Physics*. [doi:10.1063/1.3614525]

I. INTRODUCTION

Photothermal radiometry (PTR) is a nondestructive remote sensing technique that has been widely used to measure the thermal diffusivity of homogeneous samples. Since the seminal work by Mandelis and co-workers,[1] modulated PTR has also been used for thermal conductivity depth profile reconstruction of heterogeneous samples as case (surface) hardened steels,[2–7] functionally graded materials,[8] and partially cured dental resins.[9] In the last years, two works dealing with the application of modulated PTR to the simultaneous reconstruction of the in-depth varying absorption coefficient (α) and thermal diffusivity (D) of semitransparent heterogeneous samples have been published.[10,11]

The aim of this work is to study the capability of modulated PTR to obtain simultaneously α and D in multilayered materials. First, we apply the thermal quadrupole method to calculate the surface temperature of layered semitransparent materials. The thermal quadrupole method is a unified exact method for representing linear systems. It has been applied in the framework of heat conductive transfer to calculate the surface temperature of opaque multilayered samples[12] and to calculate the combined radiative and conductive heat transfer in semitransparent bulk materials.[13] Here, we extend this elegant matrix method to express the surface temperature of multilayered semitransparent samples in a compact manner. Plane and Gaussian illuminations are studied. We focus on the following issues: (a) the influence of heat losses by convection and radiation in the modulated PTR signal, (b) the influence of the thin paint layers, that are used to increase the light absorptivity and infrared emissivity, on the accuracy of the thermal diffusivity measurements, using modulated PTR, (c) the effect of lateral heat diffusion due to the use of Gaussian laser beams, and (d) the retrieval of the thermal contact resistance in glass stacks. Modulated PTR measurements confirm the validity of the model.

Finally, we address the simultaneous reconstruction of α and D depth profiles in heterogeneous materials with continuously varying physical properties. These materials are modeled as stratified ones made of a large number of parallel layers, each one characterized by constant α and D. In this work, sigmoidal α and D profiles are studied, although similar results are obtained for exponential profiles. The procedure is as follows: (a) we calculate the amplitude and phase of the surface temperature for a given α and D sigmoidal profile using the thermal quadrupole method with a large number of layers, (b) then, we add a white uniform noise to these amplitude and phase values to simulate experimental data, and (c) finally, we apply a nonlinear-regularized minimization with a total variation (TV) penalty term[14] to reconstruct the α and D depth profiles using a different number of layers in order to avoid inverse crime, i.e., an excessively optimistic accuracy of the reconstructions.[15] The quality of the reconstructed thermal and optical depth-varying properties indicates the promising possibilities of this procedure.

II. THEORY

In this section, we develop the thermal quadrupole method for semitransparent materials. Modulated plane and focused illuminations are considered.

A. Modulated and plane illumination

Let us now consider the semitransparent multilayered sample depicted in Fig. 1, illuminated by a plane light beam

[a)]Author to whom correspondence should be addressed. Electronic mail: agustin.salazar@ehu.es.

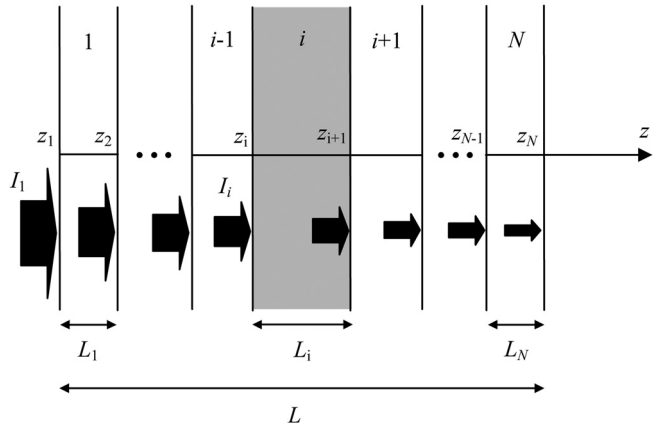

FIG. 1. Diagram of a semitransparent multilayered slab.

and modulated at a frequency f ($\omega = 2\pi f$). Each layer is characterized by its thermal conductivity (K_i), thermal diffusivity (D_i), optical absorption coefficient (α_i), and thickness (L_i). The one-dimensional (1D) heat diffusion equation for each layer writes

$$\frac{d^2T_i}{dz^2} - q_i^2 T_i = -\frac{Q_i}{K_i}, \tag{1}$$

where $q_i = \sqrt{i\omega/D_i}$ is the thermal wave vector and $Q_i = \frac{I_i}{2}\alpha_i e^{-\alpha_i(z-z_i)}$ is the heat source. I_i is the incident light intensity reaching layer i that, in the absence of internal reflections, is given by $I_i = I_1 e^{-(\alpha_1 L_1 + \alpha_2 L_2 + \ldots + \alpha_{i-1} L_{i-1})}$. The solution of Eq. (1) is usually expressed by exponential functions[16]

$$T_i(z) = A_i e^{q_i(z-z_i)} + B_i e^{-q_i(z-z_i)} + C_i e^{-\alpha_i(z-z_i)}, \tag{2}$$

where A_i and B_i are constants obtained from the boundary conditions and

$$C_i = \frac{I_i \alpha_i}{2K_i\left(q_i^2 - \alpha_i^2\right)}. \tag{3}$$

However, when dealing with the thermal quadrupole method, it is more convenient to use hyperbolic functions:

$$T_i(z) = A_i Sinh[q_i(z-z_i)] + B_i Cosh[q_i(z-z_i)] + C_i e^{-\alpha_i(z-z_i)}, \tag{4a}$$

$$\begin{aligned}\phi_i(z) &= -K_i \frac{dT_i}{dz} \\ &= -K_i q_i \{A_i Cosh[q_i(z-z_i)] + B_i Sinh[q_i(z-z_i)]\} \\ &\quad + K_i C_i \alpha_i e^{-\alpha_i(z-z_i)},\end{aligned} \tag{4b}$$

where ϕ is the heat flux.

By applying Eq. (4) at the front (z_i) and rear (z_{i+1}) surfaces of layer i, a matrix relationship between temperature and heat flux at both surfaces is obtained:

$$\begin{pmatrix} T_i(z_i) \\ \phi_i(z_i) \end{pmatrix} = \begin{pmatrix} a_i & b_i \\ c_i & d_i \end{pmatrix} \begin{pmatrix} T_i(z_{i+1}) - X_i \\ \phi_i(z_{i+1}) - Y_i \end{pmatrix}, \tag{5}$$

where $a_i = d_i = Cosh(q_i L_i)$, $b_i = \frac{Sinh(q_i L_i)}{K_i q_i}$, $c_i = K_i q_i Sinh(q_i L_i)$, $X_i = C_i\left[\frac{\alpha_i}{q_i} Sinh(q_i L_i) - Cosh(q_i L_i) + e^{-\alpha_i L_i}\right]$, and

$$Y_i = C_i K_i \left[q_i Sinh(q_i L_i) - \alpha_i Cosh(q_i L_i) + \alpha_i e^{-\alpha_i L_i}\right].$$

According to Eq. (5), the temperatures at the front and rear surfaces of layer i can be obtained provided the heat fluxes at its surfaces are known. Note that, if the layer is opaque, then $X_i = Y_i = 0$.

B. Modulated and focused illumination

Now, we study the same semitransparent multilayered sample as in the previous subsection, but illuminated by a modulated and focused laser beam of Gaussian profile. According to the radial symmetry of the problem, the two-dimensional (2D) heat diffusion equation for each layer writes

$$\frac{\partial^2 T_i}{\partial r^2} + \frac{1}{r}\frac{\partial T_i}{\partial r} + \frac{\partial^2 T_i}{\partial z^2} - q_i^2 T_i = -\frac{Q_i}{K_i}, \tag{6}$$

where $Q_i = \frac{2P_i e^{-(2r^2/a^2)}}{\pi a^2}\alpha_i e^{-\alpha_i(z-z_i)}$ is the heat source. P_i is the incident power reaching layer i that, in the absence of reflection, is given by $P_i = P_1 e^{-(\alpha_1 L_1 + \alpha_2 L_2 + \ldots + \alpha_{i-1} L_{i-1})}$ and a is the laser beam radius (at $1/e^2$ of the intensity). The solution of Eq. (6) is obtained by using the Hankel transform[17]

$$\begin{aligned}T_i(r,z) &= \int_0^\infty \delta J_o(\delta r)\bar{T}_i(\delta,z)d\delta \\ &= \int_0^\infty \delta J_o(\delta r)\left[A_i' e^{\beta_i(z-z_i)}\right. \\ &\quad \left. + B_i' e^{-\beta_i(z-z_i)} + C_i' e^{-\alpha_i(z-z_i)}\right]d\delta\end{aligned} \tag{7}$$

where $\bar{T}_i(\delta,z)$ is the Hankel transform of the temperature, J_o is the Bessel function of zeroth order and $\beta_i^2 = q_i^2 + \delta^2$. A_i' and B_i' are constants obtained from the boundary conditions, and

$$C_i' = \frac{P_i \alpha_i}{\pi K_i\left(\beta_i^2 - \alpha_i^2\right)} e^{-(\delta a)^2/8}. \tag{8}$$

For the sake of convenience, we will use hyperbolic functions instead of exponentials when applying the thermal quadrupole method:

$$\begin{aligned}\bar{T}_i(\delta,z) &= A_i' Sinh[\beta_i(z-z_i)] + B_i' Cosh[\beta_i(z-z_i)] \\ &\quad + C_i' e^{-\alpha_i(z-z_i)},\end{aligned} \tag{9a}$$

$$\begin{aligned}\bar{\phi}_i(\delta,z) &= -K_i \frac{d\bar{T}_i}{dz} \\ &= -K_i\beta_i\{A_i' Cosh[\beta_i(z-z_i)] + B_i' Sinh[\beta_i(z-z_i)]\} \\ &\quad + K_i C_i' \alpha_i e^{-\alpha_i(z-z_i)},\end{aligned} \tag{9b}$$

where $\bar{\phi}_i(\delta, z)$ is the Hankel transform of the normal heat flux.

By applying Eq. (9) at the front (z_i) and rear (z_{i+1}) surfaces of layer i, a matrix relationship between Hankel transforms of the temperature and heat flux at both surfaces is obtained:

$$\begin{pmatrix} \bar{T}_i(\delta, z_i) \\ \bar{\phi}_i(\delta, z_i) \end{pmatrix} = \begin{pmatrix} a_i' & b_i' \\ c_i & d_i' \end{pmatrix} \begin{pmatrix} \bar{T}_i(\delta, z_{i+1}) - X_i' \\ \bar{\phi}_i(\delta, z_{i+1}) - Y_i' \end{pmatrix}, \tag{10}$$

where $a_i' = d_i' = Cosh(\beta_i L_i)$, $b_i' = \frac{Sinh(\beta_i L_i)}{K_i \beta_i}$, $c_i' = K_i \beta_i Sinh(\beta_i L_i)$, $X_i' = C_i' \left[\frac{\alpha_i}{\beta_i} Sinh(\beta_i L_i) - Cosh(\beta_i L_i) + e^{-\alpha_i L_i} \right]$, and

$$Y_i' = C_i' K_i \left[\beta_i Sinh(\beta_i L_i) - \alpha_i Cosh(\beta_i L_i) + \alpha_i e^{-\alpha_i L_i} \right].$$

Note that, if the sample is opaque, $X_i' = Y_i' = 0$. According to Eq. (10), the Hankel transform of the temperatures at the front and rear surfaces are obtained provided the Hankel transforms of the normal heat fluxes are known.

By comparing Eqs. (5) and (10), one can realize that the expressions for the 1D temperature and the Hankel transform of the 2D temperature are the same, provided the following changes are performed: $q_i \rightarrow \beta_i$ and $I_i/2 \rightarrow P_i e^{-(\delta a)^2/8}/\pi$. Accordingly, in the remaining of this theoretical analysis, we will only explicitly refer to the plane illumination.

For an anisotropic sample, for which the heat propagation is three-dimensional, one can proceed in a similar way, but using the Fourier transform instead of the Hankel transform. Moreover, by applying the inverse Laplace transform to the modulated solutions given by Eqs. (5) and (10), the temperature rise of the sample above the ambient due to a transient illumination (Dirac pulse, step-like pulse, …) can be directly obtained.

C. A homogeneous slab

Let us start by considering the simple case of a slab of thickness L illuminated by a plane and modulated light beam of intensity I_1. If the sample is adiabatically isolated from its surroundings, $\phi(0) = \phi(L) = 0$ and the matrix expression relating the temperature at the sample surfaces writes

$$\begin{pmatrix} T(0) \\ 0 \end{pmatrix} = \begin{pmatrix} a & b \\ c & d \end{pmatrix} \begin{pmatrix} T(L) - X \\ 0 - Y \end{pmatrix}. \tag{11}$$

Note that, in these calculations, the multiple reflections of the incident light beam have not been considered. If heat losses are present, the heat fluxes at the front and rear surfaces are, respectively, $\phi(0) = -h_f T(0) - K_g q_g T(0)$ and $\phi(L) = h_r T(L) + K_g q_g T(L)$, where h_f and h_r are the combined heat transfer coefficients by radiation and convection at the front and rear surfaces, respectively. The last term in each expression is the heat flux by conduction to the surrounding gas, which is proportional to the surface temperature, since the gas is considered infinitely thick. According to Eq. (5), the matrix expression relating the temperature at the sample surfaces can be written as

$$\begin{pmatrix} T(0) \\ 0 \end{pmatrix} = \begin{pmatrix} 1 & 0 \\ h_f & 1 \end{pmatrix} \begin{pmatrix} 1 & 0 \\ K_g q_g & 1 \end{pmatrix} \begin{pmatrix} a & b \\ c & d \end{pmatrix} \begin{pmatrix} 1 & 0 \\ K_g q_g & 1 \end{pmatrix} \begin{pmatrix} 1 & 0 \\ h_r & 1 \end{pmatrix} \begin{pmatrix} T(L) \\ 0 \end{pmatrix} - \begin{pmatrix} 1 & 0 \\ h_f & 1 \end{pmatrix} \begin{pmatrix} 1 & 0 \\ K_g q_g & 1 \end{pmatrix} \begin{pmatrix} a & b \\ c & d \end{pmatrix} \begin{pmatrix} X \\ Y \end{pmatrix}, \tag{12}$$

where subscript g stands for the surrounding gas. As can be seen, the influence of conduction to the gas and convection and radiation are separated in independent matrices.

Figures 2 and 3 show the influence of heat losses on the surface temperature. In all the calculations, the following parameters have been used: $D_g = 22$ mm^2/s, $K_g = 0.026$ Wm^{-1}K^{-1}, and $h_f = h_r = 15$ Wm^{-2}K^{-1}, which is a good upper estimation for room temperature measurements.[18] Two normalization procedures have been analyzed. In the case of self-normalization, the ratio of the front and rear surface temperatures is considered: $T_n = T(L)/T(0)$. This is a suitable method for thin slabs. In Fig. 2, the natural logarithm of the self-normalized temperature amplitude, Ln(T_n), and its phase, $\Psi(T_n)$, are plotted against $\sqrt{f}$. Calculations have been performed for a semitransparent slab with the following parameters: $D = 0.5$ mm^2/s, $K = 1.0$ Wm^{-1}K^{-1}, $L = 0.5$ mm, and $\alpha = 3$ mm^{-1}. The dotted lines correspond to the effect of heat losses. As it is well known, the effect of heat losses is stronger at low frequencies and for poor thermal conductors.[19] However, in self-normalization, both Ln(T_n) and $\Psi(T_n)$ converge to zero at low frequencies and, therefore, the effect of heat losses is almost negligible.

The second normalization procedure consists of comparing the sample temperature at the front surface to that of a reference: $T_n' = T(0)/T_{ref}(0)$. In Fig. 3(a), a very thick opaque slab with $D = 1.0$ mm^2/s and $K = 2.5$ Wm^{-1}K^{-1} is compared with a very thick and opaque reference sample with

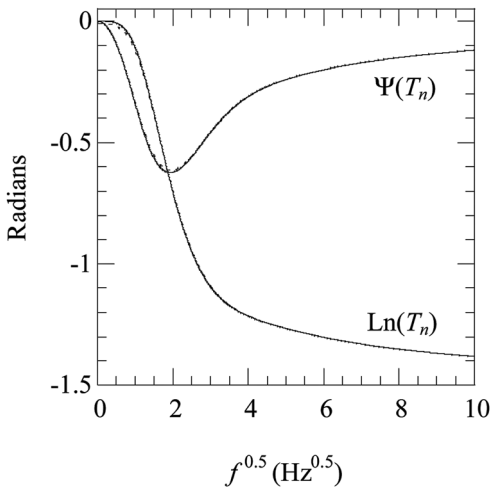

FIG. 2. Calculations of the self-normalized temperature as a function of $\sqrt{f}$ for a slab with $D = 0.5$ mm^2/s, $K = 1.0$ Wm^{-1}K^{-1}, $L = 0.5$ mm, and $\alpha = 3$ mm^{-1}. Continuous lines correspond to the absence of heat losses. Dotted lines correspond to the effect of heat losses with $h_f = h_r = 15$ Wm^{-2}K^{-1}.

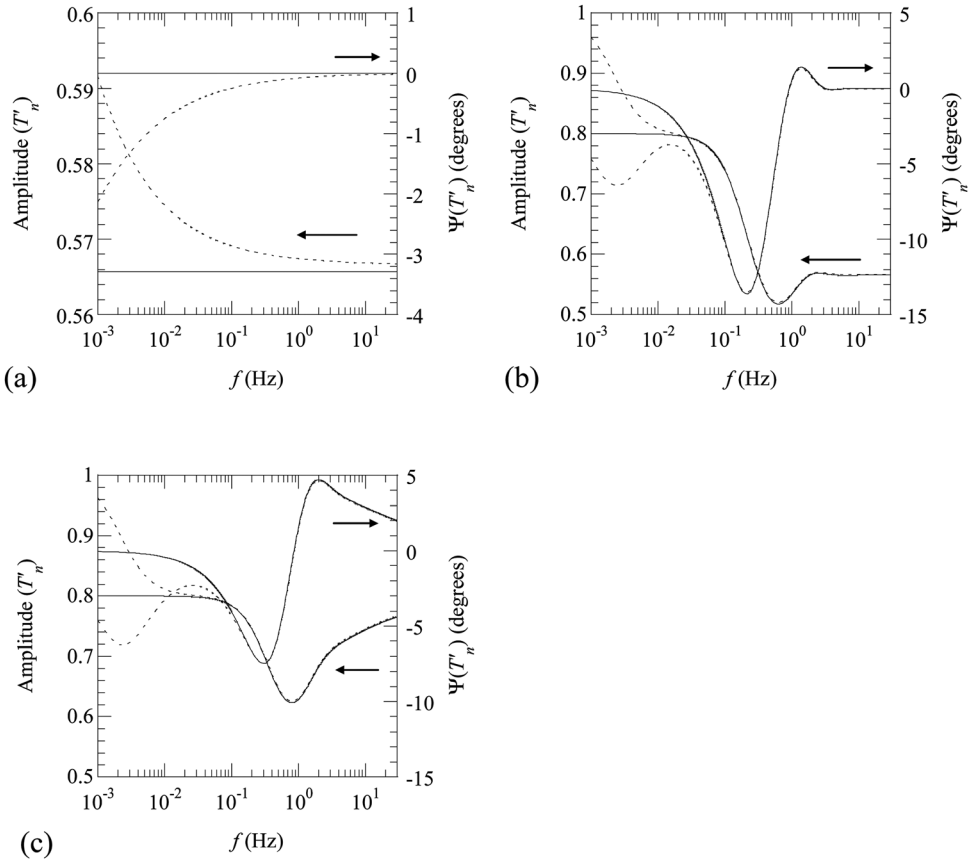

FIG. 3. Calculations of the normalized temperature with a reference with the following data: $D_{ref} = 0.5$ mm^2/s, $K_{ref} = 1.0$ Wm^{-1}K^{-1}, $D = 1.0$ mm^2/s, $K = 2.5$ Wm^{-1}K^{-1}. (a) Both are opaque and thick, (b) both are opaque and $L_{ref} = L = 1$ mm, and (c) both are semitransparent, $\alpha_{ref} = \alpha = 3$ mm^{-1}, and $L_{ref} = L = 1$ mm. Continuous lines correspond to the absence of heat losses, while dotted lines correspond to the effect of heat losses with $h_f = h_r = 15$ Wm^{-2}K^{-1}.

$D_{ref} = 0.5$ mm^2/s and $K_{ref} = 1.0$ Wm^{-1}K^{-1}. The dotted lines correspond to the deviation due to heat losses. As can be seen, only at frequencies below 0.1 Hz must the influence of heat losses be taken into account. Note that, in absence of heat losses, the amplitude of T'_n is equal to $e_{ref}/e = 0.566$, where $e = K/\sqrt{D}$ is the thermal effusivity and $\Psi(T'_n) = 0$. This means that, if the sample and the reference are thermally thick, only the thermal effusivity of the sample can be obtained.

In Fig. 3(b), we show the same calculations as in Fig. 3(a), but $L_{ref} = L = 1$ mm. As before, the dotted lines indicate the effect of heat losses, which are negligible above 0.1 Hz. Note that the amplitude of T'_n converges to $e_{ref}/e = 0.566$ at high frequencies and to $(\rho cL)_{ref}/(\rho cL) = 0.80$ at low frequencies, where $\rho c = K/D$ is the heat capacity. In its turn, $\Psi(T'_n)$ converges to zero, both at low and high frequencies. From the shape of the normalized temperature at intermediate frequencies, both D and K can be retrieved.

Finally, in Fig. 3(c), we show the same calculations as in Fig. 3(b), but for semitransparent sample and reference, with $\alpha_{ref} = \alpha = 3$ mm^{-1}. As can be seen, the information on the optical properties appears at frequencies higher than 0.1 Hz, where the effect of heat losses is negligible.

As the effect of heat losses is only significant below 0.1 Hz and most experimental measurements with modulated PTR are performed at frequencies above this limit, heat losses will not be considered in the remainder of the manuscript.

D. A multilayered material

The powerfulness of the matrix method is more evident when dealing with multilayered structures. We come back to the multilayered sample depicted in Fig. 1. For the sake of simplicity, Eq. (5) can be expressed as

$$H_i = M_i(O_i - P_i), \tag{13}$$

where H_i is the input matrix, O_i is the output matrix, M_i is the thermal matrix, and P_i is the optical matrix. To obtain a single matrix equation, relating temperature and heat flux at the front ($z = z_1 = 0$) and rear ($z = z_{N+1} = L$) surfaces, we need to know the relationship between temperature and heat flux at each intermediate boundary. Two possibilities are considered:

(a) If there is a perfect thermal contact between the layers, temperature and heat flux continuity can be applied: $T_i(z_{i+1}) = T_{i+1}(z_{i+1})$ and $\phi_i(z_{i+1}) = \phi_{i+1}(z_{i+1})$, and, therefore, $O_i = H_{i+1}$. By applying this equation to each layer, we obtain

$$H_1 = \mathbb{Z}_N O_N - \sum_{p=1}^{N} \mathbb{Z}_p P_p, \tag{14}$$

where $\mathbb{Z}_p = \prod_{i=1}^{p} M_i$, $H_1 = \begin{pmatrix} T_1(0) \\ \phi_1(0) \end{pmatrix}$, and $O_N = \begin{pmatrix} T_N(L) \\ \phi_N(L) \end{pmatrix}$. If heat losses are negligible, $\phi_1(0) = \phi_N(L) = 0$.

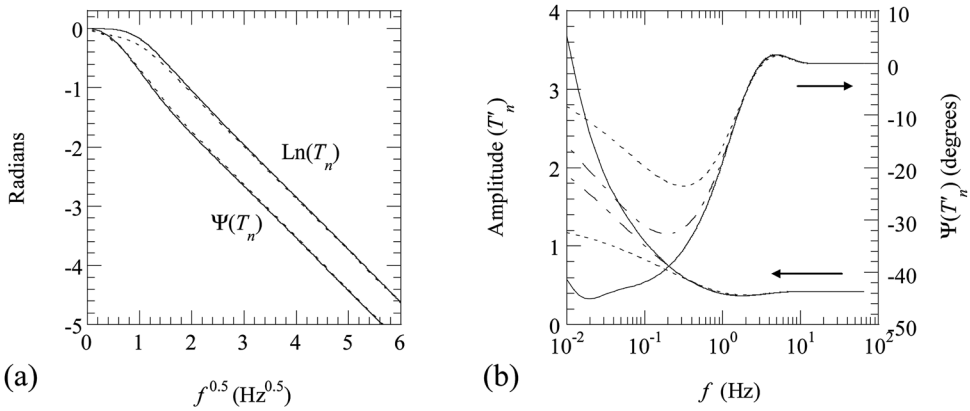

FIG. 4. Influence of the laser spot size on the normalized temperature for a stainless steel slab ($D=4.0$ mm^2/s, $K=15.0$ Wm^{-1}K^{-1}, $L=1.0$ mm). (a) Self-normalized temperature and (b) normalization with reference (vitreous carbon: $D=6.0$ mm^2/s, $K=6.3$ Wm^{-1}K^{-1}, $L=\infty$). $a=\infty$ (continuous lines), $a=10$ mm (dashed lines), and $a=5$ mm (dotted lines).

(b) A thermal resistance $R_{i,i+1}$ is introduced to account for the lack of adherence between the layers i and $i+1$. This means that the heat flux continuity still holds but there is a jump in temperature given by $T_i(z_{i+1}) = T_{i+1}(z_{i+1}) + R_{i,i+1}\phi_{i+1}(z_{i+1})$, and, therefore, $O_i = \Re_{i,i+1}H_{i+1}$, where $\Re_{i,i+1} = \begin{pmatrix} 1 & R_{i,i+1} \\ 0 & 1 \end{pmatrix}$. This means that the matrix equation relating temperature and heat flux at the front ($z=0$) and rear ($z=L$) surfaces are similar to Eq. (14), but changing $\mathbb{Z}_p$, that is the product of the thermal matrices, by $\mathbb{Z}'_p = M_1\Re_{1,2}M_2\Re_{2,3}M_3, \ldots\ldots, M_{p-1}\Re_{p-1,p}M_p$,

$$H_1 = \mathbb{Z}'_N O_N - \sum_{p=1}^{N} \mathbb{Z}'_p P_p. \tag{15}$$

III. APPLICATIONS

As this paper deals with modulated and plane illumination, we first analyze the effect of using a Gaussian laser beam instead of a completely flat light source, i.e., the disturbing effect of 2D heat propagation. Simulations are performed for a stainless steel slab ($D=4.0$ mm^2/s, $K=15.0$ Wm^{-1}K^{-1}, $L=1.0$ mm). In Fig. 4(a), we show the self-normalized amplitude and phase as a function of the square root of the frequency. The continuous line corresponds to a plane light beam, and the dotted line corresponds to a Gaussian beam with $a=5$ mm. As can be seen, the influence of the lateral heat diffusion in the slopes and, therefore, in the thermal diffusivity of the steel sample is almost negligible. In Fig. 4(b), we show the result of the normalization of the steel sample with a reference made of vitreous carbon ($D=6.0$ mm^2/s, $K=6.3$ Wm^{-1}K^{-1}, $L=\infty$). The continuous lines stand for a plane light beam, the dashed lines for $a=10$ mm, and the dotted lines for $a=5$ mm. Now, the influence of lateral heat diffusion is not negligible and, to retrieve the thermal properties of the steel sample accurately, the size of the laser spot must be included in the fitting procedure.

One of the applications of this matrix method is to quantify the effect of coating the sample surfaces with paint layers in order to increase the light absorption and the IR emissivity. In Fig. 5, we show the effect of the presence of paint layers ($D_{paint}=0.20$ mm^2/s and $K_{paint}=0.40$ Wm^{-1}K^{-1}) of different thicknesses in the self-normalized temperature of a Ni slab 1.03 mm thick ($D_{Ni}=22$ mm^2/s and $K_{Ni}=80$ Wm^{-1}K^{-1}) using plane illumination. In the absence of the paint layers, continuous lines Ln(T_n) and $\Psi(T_n)$ are parallel straight lines from whose slope (m) the thermal diffusivity can be obtained: $m=-L\sqrt{\pi/D}$. The presence of two 1 μm thick paint layers (open circles) produces an increase of the slope, leading to an underestimation of the thermal diffusivity of the material if the above equation is directly applied, i.e., using $L=L_{sample}+L_{paint}$. For 10 μm thick paint layers (crosses), even the parallelism of Ln(T_n) and $\Psi(T_n)$ is lost. This is the reason why we obtained smaller values of the thermal diffusivity of Ni and AISI-304 stainless steel than those found in the literature (see Table I in the first part of this paper). In Fig. 6(a), we quantify the error in the thermal diffusivity of opaque slabs due to the presence of the thin paint layers as a function of the diffusivity of the sample. As before, the slope $m=-L\sqrt{\pi/D}$ is used to calculate the thermal diffusivity, where L is the sum of the thickness of the sample and the thicknesses of the two paint layers.

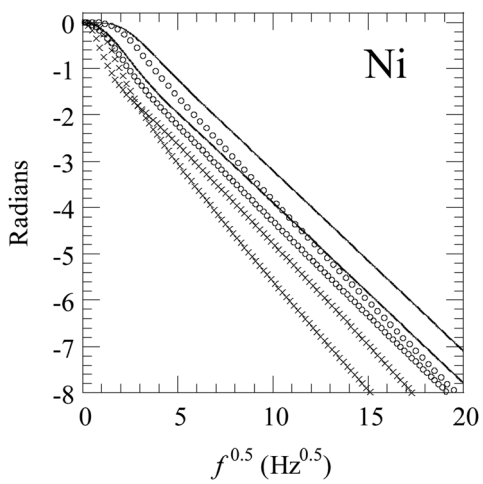

FIG. 5. Calculations of the self-normalized temperature as a function of $\sqrt{f}$ for a Ni slab 1.03 mm thick with paint layers in each surface using plane illumination. Continuous lines $L_{paint}=0$, open circles $L_{paint}=1$ μm, and crosses $L_{paint}=10$ μm. Upper and lower curves correspond to Ln(T_n) and $\Psi(T_n)$, respectively.

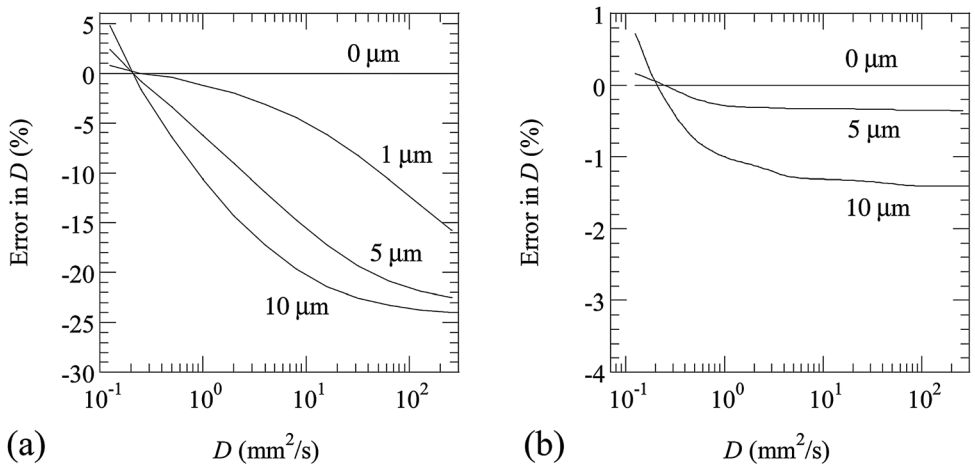

FIG. 6. (a) Simulation of the error in the thermal diffusivity of opaque slabs due to the presence of a thin paint layer as a function of the thermal diffusivity using modulated PTR. (b) The same using the flash method. Results for paint layers of 1 μm, 5 μm, and 10 μm are shown.

Calculations have been performed for various thicknesses of the paint layers, whose thermal properties are: $D_{paint} = 0.20$ mm^2/s and $K_{paint} = 0.40$ Wm^{-1}K^{-1}. In all the calculations, the ratio $L/\sqrt{D} = 0.5\text{s}^{0.5}$ is kept constant. In this figure, it can be seen that, the further the thermal diffusivities of paint and sample, the higher the error on the obtained thermal diffusivity of the sample. Note that even a 1 μm thick paint layer can produce a significant error on thermal diffusivity measurements. Moreover, these calculations show that using a coating of higher/lower thermal diffusivity than that of the sample introduces an overestimation/underestimation on the retrieved sample diffusivity. In particular, paint layers must be avoided for accurate modulated PTR thermal diffusivity measurements of good thermal conductors. Anyway, it is surprising that, in the laser flash method, where the front surface of an opaque plate is illuminated by a brief light pulse and the temperature at the rear surface is recorded, the influence of the paint layers is almost negligible (see Fig. 6(b)).

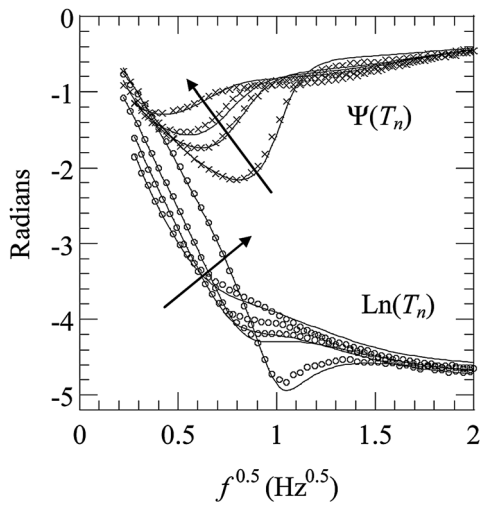

FIG. 7. Modulated PTR measurements of the self-normalized temperature as a function of $\sqrt{f}$ for a filter stack made of two equal neutral density filters ($L = 1.04$ mm) with a holed plastic film as a barrier. Plane illumination has been used. The thickness of the plastic film is varied: 0 (no plastic), 25 μm, 50 μm, and 75 μm. The arrows indicate increasing thicknesses of the plastic films. Continuous lines are the fittings to Eq. (15).

A second application is the characterization of the thermal contact resistance between layers. In Fig. 7, we show by symbols the self-normalized PTR signal corresponding to a two-layer sample made of two neutral density filters (Edmund Optics, optical density 1.0) of the same thickness, $L = 1.04$ mm, whose properties were measured in the first part of this paper ($D = 0.54$ mm^2/s, $\alpha = 2.10$ mm^{-1}, and $\beta = \infty$). These modulated PTR measurements have been performed using the same experimental setup as in Part I of this work, using plane illumination. In order to vary the thermal contact resistance, a plastic layer with a centered hole of 2 cm of diameter was placed between the two glass slabs. Plastic films of the following thicknesses were used: 0 (no plastic film), 25 μm, 50 μm, and 75 μm. The glass slabs with the plastic films were pressed using two clips. The continuous lines correspond to the simultaneous fitting of Ln(T_n) and $\Psi(T_n)$ to Eq. (15), with the thermal resistance R as the fitting parameter. As can be seen, the quality of the fitting is good, and the retrieved thermal resistances are 1.05×10^{-4}, 7.6×10^{-4}, 1.6×10^{-3}, and 2.3×10^{-3} Km^2 W^{-1}. According to the expression $R = L/K_{air}$, where $K_{air} = 0.026$ Wm^{-1}K^{-1}, these thermal resistances correspond to air layers of thickness 2.7 μm (no plastic film), 20 μm, 41 μm, and 60 μm, which are close to, but a bit below, the geometrical values. This underestimation could be ascribed to the real reduction of the air layer, since the clamping decreases the plastic film thickness.

Finally, we deal with the simultaneous reconstruction of D and α in materials with in-depth varying physical properties, as is the case of partially cured resins and functionally graded materials.[20] In this work, we present the results for sigmoidal α and D profiles, although similar conclusions have been obtained for exponential and oscillating profiles. The continuous lines in Fig. 8 show typical α and D in-depth profiles for partially cured dental resins.[11] Due to photopolymerization, the thermal diffusivity of the resin increases, while the optical absorption coefficient decreases, i.e., the material becomes a better thermal conductor and more transparent. In this process, the heat capacity is assumed to remain constant: $\rho c = 2.5 \times 10^6$ Jm^{-3}K^{-1}. In the example of Fig. 8, the curing process reaches about 0.3 mm. As can be

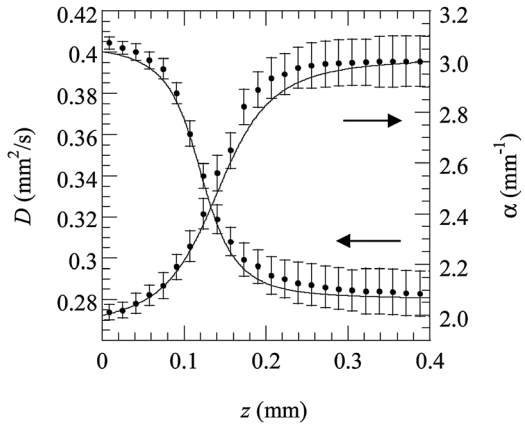

FIG. 8. Real sigmoidal diffusivity and absorption coefficient profiles (continuous lines) and reconstructed profiles using the TV regularization (dots).

seen, the shape of $D(z)$ and $\alpha(z)$ are not exactly anticorrelated, in order to study the most general and difficult case (if we had the *a priori* information that they are completely anticorrelated, the problem would reduce to reconstruct one of them). In Fig. 9, we show by symbols the normalized amplitude and phase of the surface temperature. A white uniform noise has been added to simulate the experimental data: $\pm 1\%$ in amplitude and $\pm 0.25^\circ$ in phase. The synthetic data have been obtained using the thermal quadrupole method, Eq. (14), using 1000 layers. Normalization is performed with a completely cured sample, i.e., $D = 0.40$ mm^2/s and $\alpha = 2$ mm^{-1}. In these calculations, the sample is assumed to be opaque to IR wavelengths. These synthetic data have been used to reconstruct the α and D profiles. The total variation (TV) method has been used, since it is more efficient to reconstruct steep sigmoidal shapes than Tikhonov regularization. Details of the inverse procedure are given in Ref. 21. The continuous lines in Fig. 9 correspond to the best fitting of the synthetic data using TV method. On the other hand, the dots in Fig. 8 are the mean value of the reconstructed α and D profiles at each depth. The error bar is related to the different reconstructions obtained from different initial guesses. As can be seen, the quality of the reconstruction of

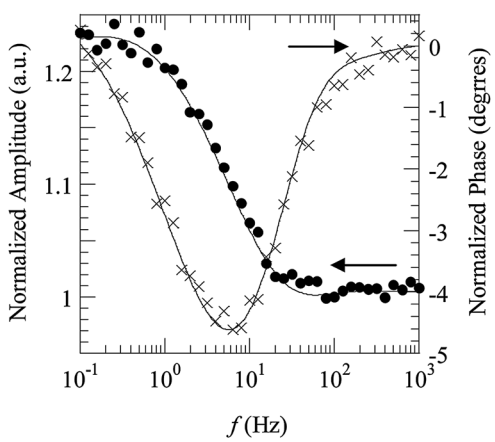

FIG. 9. Normalized amplitude (dots) and phase (crosses) synthetic values of the surface temperature corresponding to the D and α profiles of Fig. 8. White noise has been added to simulate experimental data. Solid lines are the best fittings using TV regularization.

both D and α is quite good, indicating the ability of photothermal techniques to retrieve not only the in-depth varying thermal properties, but also the optical properties.

IV. SUMMARY AND CONCLUSIONS

In this work, we have extended the thermal quadrupole method to semitransparent multilayered structures, including the cases of plane and focused illuminations. We have analyzed important experimental aspects, like heat losses, 2D propagation, and coating of the sample, that affect the values of thermal diffusivity and optical absorption coefficient obtained from PTR data. The analysis has been carried out, both when performing self-normalization and when using normalization with a reference sample. In self-normalization, the influence of both heat losses and 2D heat propagation is negligible. However, when using the normalization with a reference, both effects must be taken into account. On the one hand, heat losses are important only at frequencies below 0.1 Hz and, therefore, in most experimental conditions, their influence can be neglected. On the contrary, the effect of 2D heat propagation is more significant, and it can influence greatly the accuracy of the retrieved thermal and optical parameters. In order to overcome this issue, a laser with a top hat shape is the best option. Otherwise, 2D heat propagation must be used in the fitting procedure, where the size of the Gaussian beam must be included. The analysis also shows that paint layers as thin as 1 μm can significantly affect the thermal diffusivity of opaque materials obtained from PTR data in cases where the diffusivities of the coating and the sample are very different. For this reason, the use of very thin (nm thick) coating layers is advised, in case the optical absorption or IR emissivity of the sample needs to be improved.

Finally, the ability of the method to assess thermal resistances has been validated experimentally by evaluating the air thickness between two glasses from PTR data. The good agreement between the retrieved air gap thicknesses and the actual distance between glasses confirms the validity of the model. Moreover, the application of the method to retrieve simultaneously in-depth varying thermal diffusivity and absorption coefficient profiles from synthetic data has given very promising results. Experimental measurements on partially cured dental resins and on functionally graded materials are now in progress to verify the validity of the procedure.

ACKNOWLEDGMENTS

This work has been supported by the Ministerio de Educación y Ciencia (MAT2008-01454) and by Gobierno Vasco (Saiotek-2010/00023).

[1]M. Munidasa, T.-C. Ma, A. Mandelis, S. K. Brown, and L. Mannik, Mater. Sci. Eng., A **159**, 111 (1992).
[2]T. T. N. Lan, U. Seidel, H. G. Walther, G. Goch, and B. Schmitz, J. Appl. Phys. **78**, 4108 (1995).
[3]L. Nicolaides, A. Mandelis, and C. J. Beingessner, J. Appl. Phys. **89**, 7879 (2001).
[4]H. G. Walther, D. Fournier, J. C. Krapez, M. Luukkala, B. Schmitz, H. Stamm, and J. Thoen, Anal. Sci. **17**, s165 (2001).

[5]S. Paoloni, P. Mayr, C. Glorieux, R. Li Voti, H. Bentefour, and J. Thoen, Anal. Sci. **17**, s406 (2001).
[6]C. Wang and A. Mandelis, Rev. Sci. Instrum. **78**, 054902 (2007).
[7]H. Qu, C. Wang, X. X. Guo, and A. Mandelis, J. Appl. Phys. **104**, 113518 (2008).
[8]Y. Nagasaka, T. Sato, and T. Ushiku, Meas. Sci. Technol. **12**, 2081 (2001).
[9]P. Martínez-Torres, A. Mandelis, and J. J. Alvarado-Gil, J. Appl. Phys. **106**, 114906 (2009).
[10]J. Ravi, Y. Lu, S. Longuemart, S. Paoloni, H. Pfeiffer, J. Thoen, and C. Glorieux, J. Appl. Phys. **97**, 014701 (2005).
[11]P. Martínez-Torres, A. Mandelis, and J. J. Alvarado-Gil, J. Appl. Phys. **108**, 054902 (2010).
[12]D. Maillet, S. André, J. C. Batsale, A. Degiovanni, and C. Moyne, *Thermal Quadrupoles* (Wiley, New York, 2000).
[13]S. André, B. Rémy, D. Maillet, and A. Degiovanni, J. Appl. Phys. **96**, 2566 (2004).
[14]C. R. Vogel, *Computational Methods for Inverse Problems* (SIAM, Philadelphia, 2002).
[15]D. Colton and R. Kress, *Inverse Acoustic and Electromagnetic Scattering Theory* (Springer-Verlag, Berlin, 1998), pp. 133-304.
[16]A. Rosencwaig and A. Gersho, J. Appl. Phys. **47**, 64 (1976).
[17]A. Salazar, A. Sánchez-Lavega, and J. Fernández, J. Appl. Phys. **65**, 4150 (1989).
[18]A. Salazar, A. Mendioroz, and R. Fuente, Appl. Phys. Lett. **95**, 121905 (2009).
[19]G. Rousset, F. Charbonnier, and F. Lepoutre, J. Appl. Phys. **56**, 2093 (1984).
[20]Y. Miyamoto, W. A. Kaysser, B. H. Rabin, A. Kawasaki, and R. G. Ford, *Functionally Graded Materials: Design, Processing, and Applications* (Kluwer, Boston, 1999).
[21]E. Apiñaniz, A. Mendioroz, A. Salazar, and R. Celorrio, J. Appl. Phys. **108**, 064905 (2010).